Electronic Supplementary Material (ESI) for ChemComm.
This journal is © The Royal Society of Chemistry 2018

Supporting Information for:

Plutonium coordination and redox chemistry with the $CyMe_4$-BTPhen polydentate N-donor extractant Ligand

Sean D. Reilly,[a] Jing Su,[a] Jason M. Keith,[a,¥] Ping Yang,[a] Enrique R. Batista,*[,a] Andrew J. Gaunt,*[,a] Laurence M. Harwood,*[,b] Michael J. Hudson,[b,#] Frank W. Lewis,[b,c] Brian L. Scott,[a] Clint A. Sharrad*[,d] and Daniel M. Whittaker[d]

[a]*Los Alamos National Laboratory, Los Alamos, New Mexico 87545.*
[b]*Department of Chemistry, University of Reading, Whiteknights, Reading RG6 6AD, U.K.*
[c]*Department of Applied Sciences, Faculty of Health and Life Sciences, Northumbria University, Newcastle upon Tyne, NE1 8ST, U.K.*
[d]*School of Chemical Engineering and Analytical Science, The University of Manchester, Oxford Road, Manchester, M13 9PL, U.K.*

[#]*Deceased 24th January 2016.*
[¥]*Current address: Colgate University, Hamilton, New York 13346, United States*

Experimental Details.

General.

Plutonium (of predominantly ^{239}Pu isotopic composition) solutions were purified using anion-exchange chromatography to give aqueous Pu(IV) solutions in HNO_3 or HCl. The plutonium solution concentration and oxidation state were determined by measuring the vis–NIR spectrum of a solution sample diluted in 1.0 M $HClO_4$.[1]

A Varian Cary 6000i spectrophotometer with a fixed spectral bandwidth of 0.2 nm was used to record solution electronic absorption spectra at ambient temperature. Solid diffuse reflectance spectra were collected using a Varian Cary 6000i with installed Internal Diffuse Reflectance Accessory. ^1H NMR spectroscopy was performed using a Bruker Avance 300 MHz spectrometer. The ligands 2,9-bis(5,5,8,8-tetramethyl-5,6,7,8-tetrahydro-1,2,4-benzotriazin-3-yl)-1,10-phenanthroline ($CyMe_4$-BTPhen) and 6,6'-bis(5,5,8,8-tetramethyl-5,6,7,8-tetrahydro-1,2,4-benzotriazin-3-yl)-2,2'-bipyridine ($CyMe_4$-BTBP) were prepared and purified by previously published procedures, using the $CyMe_4$-BTPhen dihydrate form for the plutonium studies in this work.[2] Acids and organic solvents were purchased commercially and used as received.

Synthesis of $[Pu^{III}(CyMe_4\text{-}BTPhen)_2(NO_3)][Pu^{IV}(NO_3)_6]\cdot 4MeCN$. $[N(n\text{-}Bu)_4]_2[Pu(NO_3)_6]$ was dissolved in MeCN (1.37 mL, 25.1 μmol Pu^{IV}) and filtered to give a clear green solution, then added dropwise to a stirred suspension of $CyMe_4$-BTPhen (14.0 mg, 23.5 μmol) in 1.6 mL MeCN. The $CyMe_4$-BTPhen dissolved as the Pu was added and the solution turned from yellow to brown. This 1:1 Pu:$CyMe_4$-BTPhen solution in MeCN was gently heated for 30 min, concentrating the solution in the process. The solution was then put through a series of evaporations and redissolution procedures in an attempt to grow X-ray diffraction quality single-crystals of the product. Success was achieved by vapor diffusion of Et_2O into an MeCN (1.5 – 2.0 mL) solution of the product. Large dark brown crystals were obtained along with some light brown powder precipitate. These crystals were used for structural determination of $[Pu^{III}(CyMe_4\text{-}BTPhen)_2(NO_3)][Pu^{IV}(NO_3)_6]\cdot 4MeCN$ and also for vis-NIR characterization. The synthesis was repeated to provide fresh crystals that were used for NMR characterization.

UV–vis–NIR (diffuse reflectance, solid) λ_{max}, nm: 605, 642, 671, 779, 828, 859 (sh), 877, 912, 940, 1067, 1132.

UV–vis–NIR (in MeCN solution) λ_{max}, nm: 610, 642, 674, 783, 826 (sh), 857, 875, 910, 941, 1062, 1131.

^{1}H NMR (crystals dissolved in CD_3CN): 9.67, 8.82, 8.49, 8.05 (all 4 resonances broad, in the expected region for phenanthroline aromatic protons, 2 x 6 protons, relative integrals are 2:1:1:2, respectively), multiple broad resonances 2.0 – 1.0 (the region where C*H*$_2$ protons are observed on the cyclohexyl ring), 1.29 (exterior methyl groups in cyclohexyl ring, 4 x C*H*$_3$), -0.12 and -0.64 (possibly due to the interior 4 x C*H*$_2$ protons). A broad resonance at 2.67 ppm is also present as an impurity in freshly acquired CD_3CN, and, therefore, is disregarded as not attributable to the Pu-BTPhen complex. The NMR spectrum was acquired in CD_3CN because the crystalline complex was only sparingly soluble in non-coordinating solvents such as CD_2Cl_2, and it should also be noted that the crystals were not as soluble in CD_3CN as they appeared to be in CH_3CN, even when heated at 50 °C.

Due to the inability to definitively assign all resonances to exact and account via integration for all of the protons expected to be observed based on the crystal structure for $[Pu^{III}(CyMe_4\text{-}BTPhen)_2(NO_3)][Pu^{IV}(NO_3)_6]$, it was possible to directly crystallize the product from the NMR solution in CD_3CN and confirm that the unit cell of these crystals matched those used for full structural determination (*i.e.* to make sure that repeating the synthesis to provide an NMR sample did not inadvertently produce a different product). In addition to the unit cell matching, the X-ray data was refined to the point where molecular connectivity was established and verified to be identical to $[Pu^{III}(CyMe_4\text{-}BTPhen)_2(NO_3)][Pu^{IV}(NO_3)_6]$. This leads to the conclusion that the paramagnetism has rendered some signals unobservable and/or prevents accurate relative integral values.

Experimental methods/sample preparation for reactivity studies of $CyMe_4$-BTPhen with plutonium, followed by vis-NIR spectrophotometry. $[N(n\text{-}Bu)_4]_2[Pu(NO_3)_6]$ solids were prepared by adding 2 equiv $[n\text{-}Bu_4N][NO_3]$ to an aqueous Pu(IV)/HNO_3 solution to give green precipitates which were dissolved in MeCN (residual HNO_3 may be present in the solid). These solutions were then utilized for the addition of different equivalents of the $CyMe_4$-BTPhen ligand under different conditions of time, temperature and solvent, with the vis-NIR spectra recorded with each variable as described in the results section.

For the studies that compared Pu(IV) and Pu(III) reactions with $CyMe_4$-BTPhen, the ligand (8.4 mg, 14 μmol) was dissolved with heating in 2.7 mL of MeOH. An aqueous Pu(IV)/HCl solution (9.5 μL, 3.9 μmol Pu^{IV}) was added to a stirred 0.70 mL aliquot of the above methanolic $CyMe_4$-BTPhen solution (3.7 μmol $CyMe_4$-BTPhen). This solution was combined with a second 0.70 mL aliquot of the above methanolic $CyMe_4$-BTPhen solution. Four days later the solution was allowed to slowly evaporate to give crystals which diffracted but for which no unit cell could be obtained. An aqueous Pu(III)/HCl solution was prepared by reducing a Pu(IV)/HCl solution over mercury-zinc amalgam. Vis–NIR spectroscopy was used to determine Pu concentration and to verify complete reduction to Pu(III). A 141.8 μL aliquot of this Pu(III)/HCl solution (3.9 μmol Pu^{III}) was added to a stirred 0.70 mL aliquot of methanolic $CyMe_4$-BTPhen solution (3.7 μmol $CyMe_4$-BTPhen) and the vis–NIR spectrum was recorded immediately and again 3.5 hrs later. Again, no single crystals of X-ray diffraction quality could be obtained from this solution.

Experimental methods/sample preparation for reactivity studies of $CyMe_4$-BTBP with plutonium as followed by vis-NIR spectrophotometry. $[N(n\text{-}Bu)_4]_2[Pu(NO_3)_6]$ was dissolved in MeCN (386 μL, 10.9 μmol Pu^{IV}) and then added to a stirred yellow solution of $CyMe_4$-BTBP (5.8 mg, 10.9 μmol) in 2.0 mL MeCN, causing the resulting solution to turn a slightly darker yellow color. This 1:1 Pu:$CyMe_4$-BTBP solution was stirred at room temp and its vis–NIR spectrum was recorded at various time intervals. One day later a second equiv of $CyMe_4$-BTBP was added and the vis–NIR spectrum was again followed over time. Attempts to grow crystals by evaporation and Et_2O vapor diffusion yielded only powders and poor-quality crystals.

Additional spectrophotometric titrations of $[N(n\text{-}Bu)_4]_2[Pu(NO_3)_6]$ with $CyMe_4$-BTPhen, not fully detailed in the main manuscript text. In order to further explore the reaction of plutonium with the $CyMe_4$-BTPhen ligand in solution, vis-NIR spectra were recorded under several different reaction conditions and reagent stoichiometries.

The spectrum of $[N(n\text{-}Bu)_4]_2[Pu(NO_3)_6]$ dissolved in MeCN solution, followed by addition of aliquots of a $CyMe_4$-BTPhen solution in MeCN (Figure S1), caused the initially-green Pu solution to turn a clear yellow color. At this point, the spectra display a few changes but largely resemble

uncomplexed starting material. The solution was then stirred for 18 hrs to allow equilibrium to be reached (Figure S1, black). Subsequent heating of this solution caused the 840 nm 'impurity' peak to appear (Figure S2, green) and the peaks in the 600–700 nm region changed in relative intensity to more closely match the red spectrum of Figure S2, suggesting that heat was necessary in this case to drive complex formation. One possible reason for this observation could be proton competition that arises as a result of residual acid present from the preparation of $[N(n\text{-}Bu)_4]_2[Pu(NO_3)_6]$ (see experimental details and further comments below). Further support of this proposition is provided by addition of NH_4OH, which causes the 840 nm peak to disappear (Figure S2, blue and red). A brown powder precipitated from this solution overnight, and further attempts to filter and concentrate this solution yielded more powder with no crystalline solid. Given the relative sharpness and position of the 840 nm peak, it could be speculated that it has its origin from the presence of a Pu(VI) species. This would be consistent with the observation that after hydroxide addition neutralizes the residual acid then the Pu(VI) is reduced upon complex formation with $CyMe_4$-BTPhen, which favors an oxidation state of Pu(III).

In a separate follow-up experiment, $[N(n\text{-}Bu)_4]_2[Pu(NO_3)_6]$ and 1 equiv of $CyMe_4$-BTPhen were combined in MeCN and the vis-NIR spectrum was recorded at various times (Figure S3 dark blue and red traces). A second equiv of $CyMe_4$-BTPhen was then added and the spectrum was again recorded at various times (Figure S3 light blue, pink and black traces). After 6 days, the solution was heated before addition of a third $CyMe_4$-BTPhen equiv (Figure S4). While the addition of the second equiv of $CyMe_4$-BTPhen causes the peaks centered at 580–680, 780 and 940 nm to increase in intensity and the $[Pu(NO_3)_6]^{2-}$ peak at 744 nm to disappear, the third equiv of $CyMe_4$-BTPhen does not cause similar increase in peak intensity, suggesting a 1:2 complex is the limiting species, as has been previously observed in Cm(III) and lanthanide(III) complexation studies with $CyMe_4$-BTPhen.[2,3]

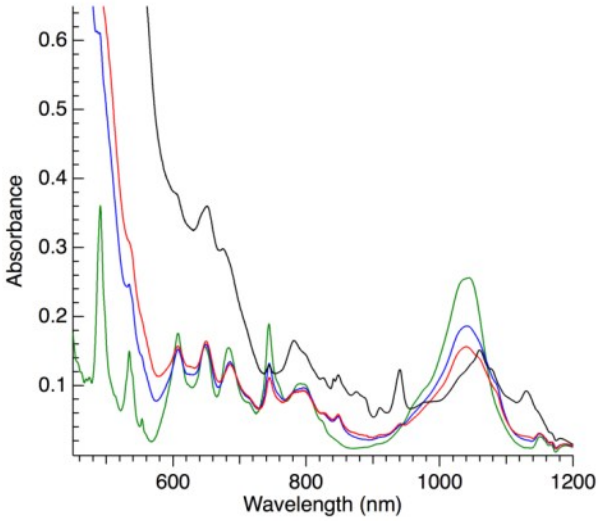

Figure S1. Spectrophotometric titration of $CyMe_4$-BTPhen into a $[N(n\text{-}Bu)_4]_2[Pu(NO_3)_6]$/MeCN solution. Electronic absorption spectra of 6.9 mM $[N(n\text{-}Bu)_4]_2[Pu(NO_3)_6]$ dissolved in MeCN (green), 0.8 equiv $CyMe_4$-BTPhen added (blue, 5.1 mM Pu), 1.6 equiv $CyMe_4$-BTPhen added (red, 4.0 mM Pu), and final solution after stirring 18 hrs at room temp (black).

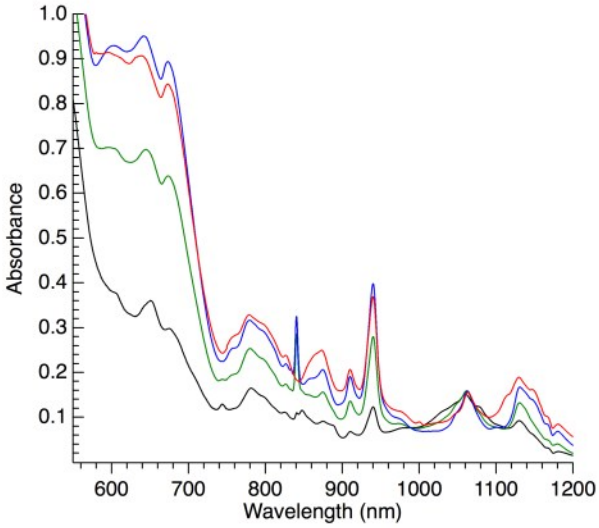

Figure S2. Solution electronic absorption spectra of 1:1.6 Pu:$CyMe_4$-BTPhen in MeCN before and after heating and adding NH_4OH. Black: Before heating (5.1 mM Pu). Green: After heating. Blue: 40 eq. NH_4OH added (relative to Pu). Red: 50 equiv NH_4OH added.

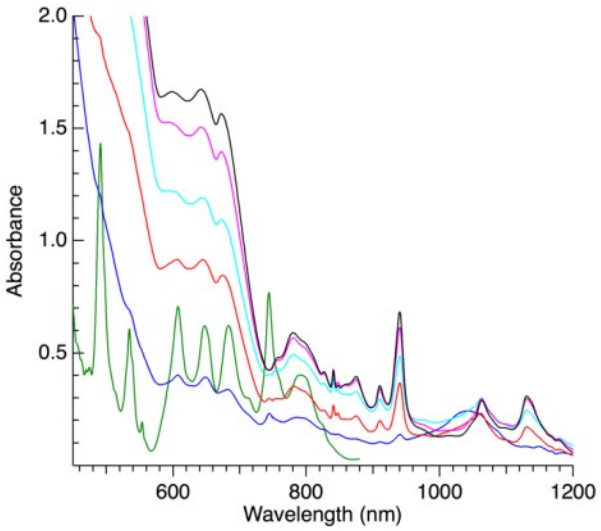

Figure S3. Solution electronic absorption spectra of $[N(n\text{-}Bu)_4]_2[Pu(NO_3)_6]$ in MeCN before and at various times after adding 1 and then 2 equiv $CyMe_4$-BTPhen. Green: 28.1 mM $[N(n\text{-}Bu)_4]_2[Pu(NO_3)_6]$ in MeCN. Dark blue: 1:1 Pu:$CyMe_4$-BTPhen immediately after mixing (5.3 mM Pu). Red: Same 1:1 solution 1 day later. Light blue: 1:2 Pu:$CyMe_4$-BTPhen immediately after adding second equiv $CyMe_4$-BTPhen (5.3 mM Pu). Pink: Same 1:2 solution 1 day later. Black: Same 1:2 solution 6 days later.

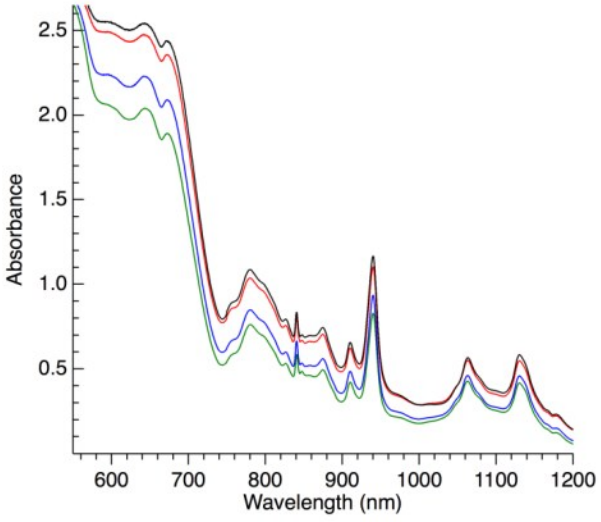

Figure S4. Solution electronic absorption spectra of Pu:$CyMe_4$-BTPhen in MeCN before and after adding 3rd equiv $CyMe_4$-BTPhen. Green: 1:2 Pu:$CyMe_4$-BTPhen before heating (~6.6 mM Pu).

Blue: Same 1:2 solution after heating. Red: 1:3 Pu:$CyMe_4$-BTPhen immediately after adding third equiv $CyMe_4$-BTPhen. Black: Same 1:3 solution 3 hrs later.

A UV–vis titration of Pu into $CyMe_4$-BTPhen in acetonitrile provided further support for 1:2 Pu:$CyMe_4$-BTPhen complex formation (Figure S5). $CyMe_4$-BTPhen dissolved in acetonitrile exhibits absorbance maxima at 261 and 295 nm. As the first 0.5 equiv Pu are added, the 261 nm absorbance shifts to 267 nm, the 295 nm peak drops in intensity, and isosbestic points are observed near 231, 265, and 284 nm. Further Pu additions have less effect on the spectrum but do cause the isosbestic points to disappear. This behavior is analogous to what was previously observed for trivalent lanthanides[2b] and suggests that a 1:2 Pu:$CyMe_4$-BTPhen complex forms when Pu is first added, some of which subsequently dissociates as excess Pu is added.

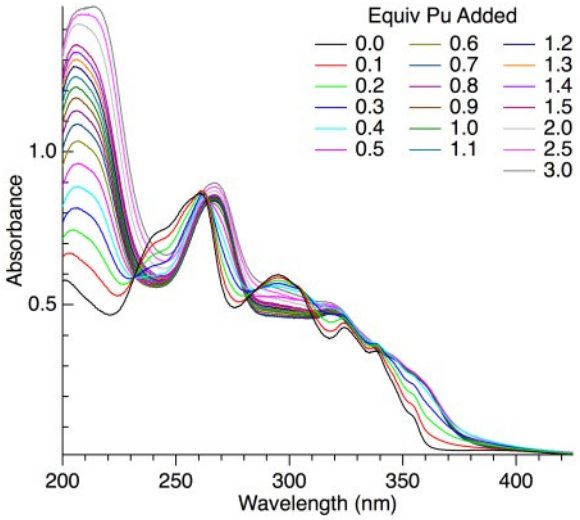

Figure S5. Solution electronic absorption spectra for the titration of 1.00 mL of 2×10^{-5} M $CyMe_4$-BTPhen with 4×10^{-4} M $[N(n\text{-}Bu)_4]_2[Pu(NO_3)_6]$ (MeCN solvent).

Over the course of our exploration of the reactivity of Pu(IV) with $CyMe_4$-BTPhen two different sources of Pu(IV) were studied. During initial studies, aqueous acidic Pu(IV) stock solutions were evaporated to dryness, redissolved in MeCN, and combined with $CyMe_4$-BTPhen solutions. These reaction solutions remained a light yellow color and vis-NIR spectra showed evidence of substantial unreacted Pu(IV). Later studies employed $[N(n\text{-}Bu)_4]_2[Pu(NO_3)_6]$ starting materials

that contained minimal residual acid. Reactions with these starting materials were much more successful. This suggests that protons and Pu cations compete for ligand nitrogen binding a low residual acid concentration favors Pu complexation.

As mentioned in the main text of the communication, in order to support assignment of the Pu oxidation state in the cation of the structure of $[Pu^{III}(CyMe_4\text{-}BTPhen)_2(NO_3)][Pu^{IV}(NO_3)_6]$, complexation of $CyMe_4$-BTPhen with Pu(III) and Pu(IV) was compared in MeOH as the primary reaction medium. A HCl source/stock solution of Pu was chosen to facilitate comparison of both oxidation states. HCl was used in these experiments because HNO_3 is incompatible with the Hg/Zn amalgam reductant used to prepare the Pu(III) stock solution (trivalent plutonium in nitric acid solution is difficult to stabilize). Aqueous Pu(IV)/HCl solution was spiked into a methanolic solution containing 1 equiv $CyMe_4$-BTPhen, causing the solution to change color from yellow to gold, and the vis–NIR spectrum was recorded over time (Figure S6). After combining with a second equiv of methanolic $CyMe_4$-BTPhen, the vis–NIR spectrum was again measured over time (Figure S6). The peak at 943 nm increases in intensity with time and the addition of a second $CyMe_4$-BTPhen equiv. While the peaks below 740 nm do not appear to change significantly in shape, they do increase in intensity. The electronic absorption profiles are different to those attributed to the Pu complexes in MeCN solution using $[Pu(NO_3)_6]^{2-}$ as the Pu(IV) precursor, but are all consistent with each other and again appear consistent with the formation of only one complex. A Pu(III)/HCl source was prepared by reduction of Pu(IV)/HCl over Hg/Zn amalgam and spiked into methanolic $CyMe_4$-BTPhen, resulting in a brown solution (Figure S7) similar in color to what is observed when $[N(n\text{-}Bu)_4]_2[Pu(NO_3)_6]$ reacts with $CyMe_4$-BTPhen in MeCN. The data does not definitively demonstrate that starting with either Pu(III) or Pu(IV) leads to identical products upon reaction with $CyMe_4$-BTPhen, but despite a few differences in the observed transitions, overall there are very similar absorbance bands that provide support for the conclusion that Pu(IV) is reduced upon complexation to the ligand. These spectra from Pu/HCl sources also allow the conclusion that the bands in the 550-750 nm region do indeed arise from Pu complexes with the $CyMe_4$-BTPhen ligand, rather than from the $[Pu(NO_3)_6]^{2-}$ starting material (the spectra from experiments described in previous sections that used the hexanitrate precursor also contain similar bands in the 550-750 nm region, which resulted in some ambiguity as to whether these were attributable to a Pu complex with the $CyMe_4$-BTPhen ligand or unreacted $[Pu(NO_3)_6]^{2-}$ anions).

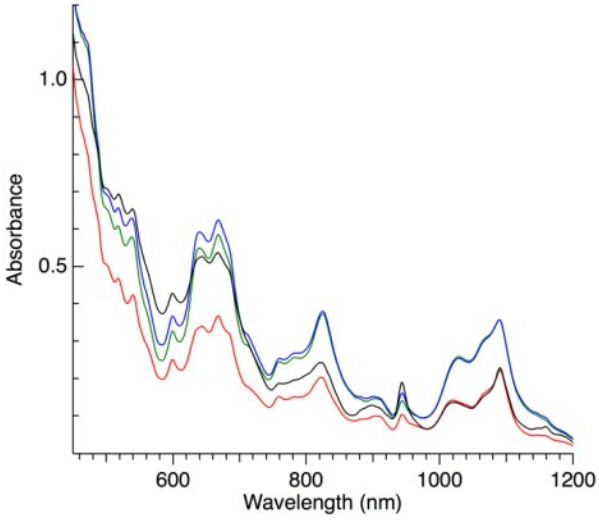

Figure S6. Solution electronic absorption spectra of the reaction of Pu(IV)/HCl with 1 and then 2 equiv $CyMe_4$-BTPhen in MeOH. Green: Intial 1:1 Pu:$CyMe_4$-BTPhen solution (5.9 mM Pu). Blue: Same 1:1 solution 3.5 hrs later. Red: 1:2 Pu:$CyMe_4$-BTPhen immediately after adding second equiv $CyMe_4$-BTPhen (2.8 mM Pu). Black: Same 1:2 solution 3 days later.

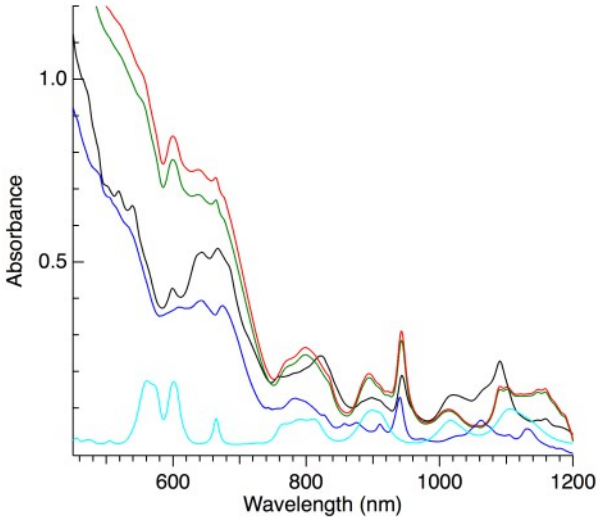

Figure S7. Solution electronic absorption spectra of the reaction of Pu(III)/HCl with 1 equiv $CyMe_4$-BTPhen in MeOH, and comparisons to Pu(IV) reactions. Light Blue: Aqueous 4.6 mM Pu(III) in 1 M HCl. Green: Intial 1:1 Pu(III):$CyMe_4$-BTPhen solution (4.6 mM Pu). Red: Same 1:1 solution 3.5 hrs later. Black: Spectrum of Pu(IV)/HCl reacted with 2 equiv $CyMe_4$-BTPhen in MeOH, 3 days after reaction started. Dark Blue: Crystals of $[Pu^{III}(CyMe_4\text{-}BTPhen)_2(NO_3)][Pu^{IV}(NO_3)_6]\cdot 4MeCN$ dissolved in MeCN (2× scaled and offset by –0.04 absorbance units for legibility).

$[N(n\text{-}Bu)_4]_2[Pu(NO_3)_6]$ $CyMe_4$-BTBP spectrophotometric titration. Previous work has demonstrated that, compared to the phenanthroline-based $CyMe_4$-BTPhen ligand, the less-rigid bipyridine-based $CyMe_4$-BTBP analog exhibits slower complex formation.[2a] Here, for comparison with $CyMe_4$-BTPhen, we followed the reaction of $[N(n\text{-}Bu)_4]_2[Pu(NO_3)_6]$ with 1 and then 2 equiv of $CyMe_4$-BTBP in MeCN by vis-NIR spectroscopy (Figure S8). Spectra recorded at the same time intervals for the reactions of $CyMe_4$-BTPhen and $CyMe_4$-BTBP with $[N(n\text{-}Bu)_4]_2[Pu(NO_3)_6]$ in MeCN were compared (Figure S9). The similar band positions suggest that the Pu coordination environment is similar for both the $CyMe_4$-BTBP and $CyMe_4$-BTPhen complexes, and that Pu(III) is also formed in the $CyMe_4$-BTBP reaction. Absorbance bands attributed to the Pu-$CyMe_4$-BTPhen complex also show a greater intensity increase after a similar reaction time, which suggests a faster initial $CyMe_4$-BTPhen reaction rate (Figure S9). These relative rates of complex

formation are consistent with previous observations. Attempts to grow crystals from the Pu-$CyMe_4$-BTBP reaction suitable for X-ray diffraction were unsuccessful.

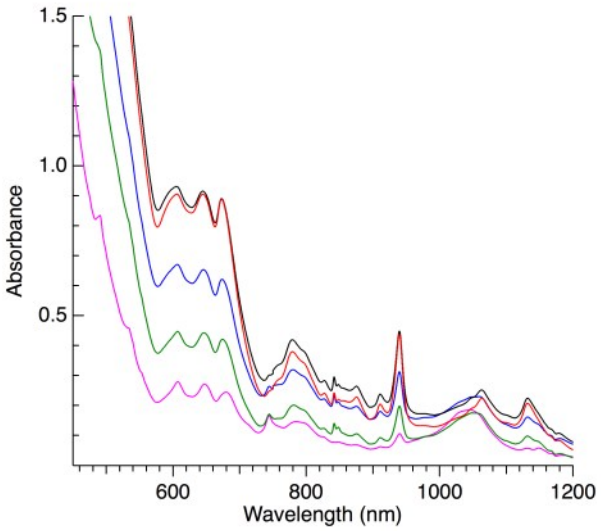

Figure S8. Solution electronic absorption spectra of 1:1 and 1:2 Pu:$CyMe_4$-BTBP in MeCN. Pink: 1:1 Pu:$CyMe_4$-BTBP immediately after mixing (4.5 mM Pu). Green: Same 1:1 solution 1 day later. Blue: 1:2 Pu:$CyMe_4$-BTBP immediately after adding second equiv $CyMe_4$-BTBP (4.5 mM Pu). Black: Same 1:2 solution 1 day later. Red: Same 1:2 solution 6 days later.

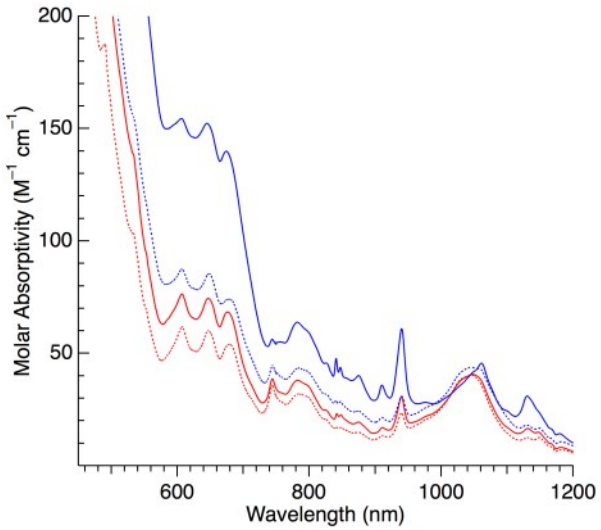

Figure S9. Solution electronic absorption spectra of the reaction of $[N(n\text{-}Bu)_4]_2[Pu(NO_3)_6]$ in MeCN with 1 equiv of $CyMe_4$-BTBP (red) or $CyMe_4$-BTPhen (blue). The dotted lines show the solutions at the start of the reaction while the solid lines are 3 hrs later. The molar absorptivity is based on the total Pu concentration in solution.

Discussion of the effect of heat on the vis/NIR spectra: The red spectrum in figure 1 of the main manuscript text showed the 1:1 Pu:$CyMe_4$-BTPhen reaction solution in MeCN immediately after the Pu(IV) metal and $CyMe_4$-BTPhen ligand solutions were combined. That spectrum is shown again as the red spectrum of Figure S10. This reaction solution was gently heated for 30 minutes, concentrating the solution in the process. The blue spectrum of Figure S10 shows what the reaction solution looked like after heating. An increase in the relative intensity of the peak at 840 nm is observed. As discussed in the main manuscript text and on page 5 of this SI, we attribute this peak to an impurity that increased after heating.

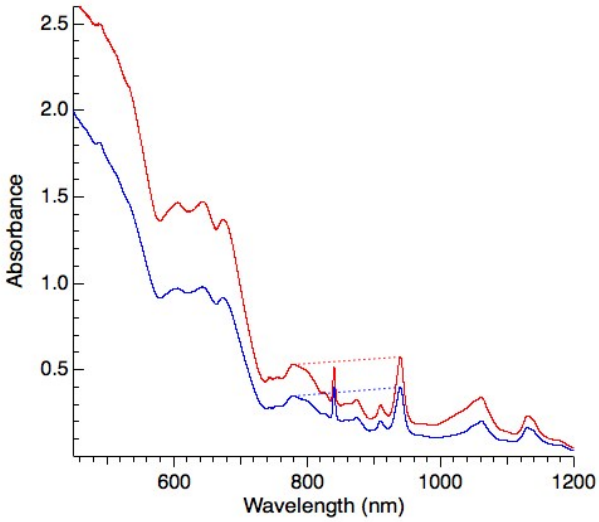

Figure S10. Solution electronic absorption spectra of 1:1 Pu:$CyMe_4$-BTPhen in MeCN before (red) and after (blue) heating showing the increased intensity of the peak at 840 nm relative to the product peaks at 780 and 940 nm after heating.

Assignment of peaks in the vis-NIR spectra of the Pu:$CyMe_4$-BTPhen reaction product. The 1:1 reaction of $[N(n\text{-}Bu)_4]_2[Pu(NO_3)_6]$ with $CyMe_4$-BTPhen in MeCN gave a solution with the vis-NIR spectrum shown as the black trace in the upper area of Figure S11 (this is the same spectrum shown as the red trace in Figure 1 of the main manuscript text). Crystals of $[Pu^{III}(CyMe_4\text{-}BTPhen)_2(NO_3)][Pu^{IV}(NO_3)_6]\cdot 4MeCN$ were obtained from this solution and subsequently redissolved in MeCN to give a solution with the vis-NIR spectrum shown as the red trace in the upper area of Figure S11 (this is the same spectrum shown as the green trace in Figure 3 of the main manuscript text). These two similar spectra were compared with a library of known Pu solution spectra in an attempt to identify the various peaks. Four relevant Pu spectra are shown in the lower area of Figure S11 for comparison.

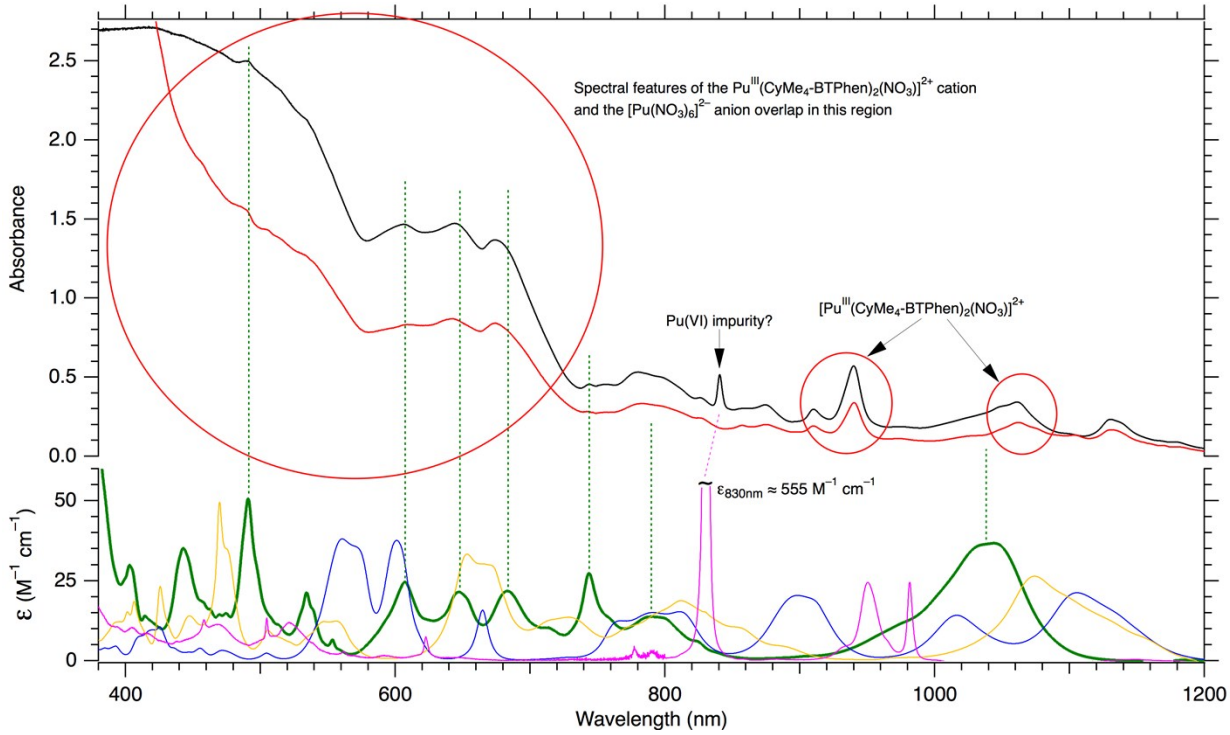

Figure S11. Annotated solution electronic absorption spectra of the 1:1 $[N(n\text{-}Bu)_4]_2[Pu(NO_3)_6]$:$CyMe_4$-BTPhen reation in MeCN. Molar aborptivities of relevant Pu solution species are shown in the lower plot area: Green: $[N(n\text{-}Bu)_4]_2[Pu(NO_3)_6]$ in MeCN. Blue: Pu(III) in aqueous 1M $HClO_4$. Yellow: Pu(IV) in aqueous 1M $HClO_4$. Magenta: Pu(VI) in aqueous 1M $HClO_4$. Solution absorption spectra of the reaction product are shown in the upper plot area: Black: 1:1 8.45 mM Pu:$CyMe_4$-BTPhen immediately after combining in MeCN. Red: solid $[Pu^{III}(CyMe_4\text{-}BTPhen)_2(NO_3)][Pu^{IV}(NO_3)_6]\cdot 4MeCN$ crystals redissolved in MeCN.

Crystal Data Acquisition. The crystal was coated in Paratone-N oil, mounted inside a 0.5 mm diameter quartz capillary, the ends sealed with capilliary wax, the exterior of the capillary coated with acrylic to provide multiple containment to mitigate the health hazards of plutonium. The reflection data were collected on a Bruker Platform diffractometer with 1k CCD, and the crystal was cooled to 140 K using a Bruker Kryoflex liquid nitrogen cryostat. The instrument was equipped with a sealed, graphite monochromatized MoKα X-ray source (λ= 0.71073 Å), and monocapillary optic. A hemisphere of data was collected using φ scans, with 30 second frame exposures and 0.3º frame widths. Data collection and initial indexing and cell refinement were handled using SMART software[4]. Frame integration, including Lorentz-polarization corrections, and final cell parameter calculations were carried out using SAINT software.[5] The data were corrected for absorption using the SADABS program.[6] Decay of reflection intensity was monitored *via* analysis of redundant frames. The structure was solved using Direct methods and difference Fourier techniques. All hydrogen atom positions were idealized, and rode on the atom they were attached to. The final refinement included anisotropic temperature factors on all non-hydrogen atoms. Structure solution, refinement, graphics, and creation of publication materials were performed using SHELXTL.[7]

Table S1. Selected single-crystal information.

	$[Pu(CyMe_4\text{-}BTPhen)_2(NO_3)][Pu(NO_3)_6]\cdot 4MeCN$
Formula	$C_{76}H_{88}N_{27}O_{21}Pu_2$
M	2193.70
Crystal System	Triclinic
a (Å)	16.109(2)
b (Å)	16.909(2)
c (Å)	18.673(3)
α (°)	63.434(2)
β (°)	79.805(2)
γ (°)	88.801(2)
Space Gp.	P-1
Z	2
T (K)	140(1)
μ (mm^{-1})	1.546
Reflns. Measd	51590
Reflns. Obsd	21029
R_1 (obsd)	0.0566
wR^2(all data)	0.1136

Density Functional Theory Calculations. Ground-state electronic structure calculations were performed on $[Pu^{IV}(NO_3)_6]^{2-}$, $[Pu^{IV}(CyMe_4\text{-}BTPhen)_2(NO_3)]^{3+}$ and $[Pu^{III}(CyMe_4\text{-}BTPhen)_2(NO_3)]^{2+}$ complexes as well as ligand/solvent (NO_3^-, $CyMe_4$-BTPhen and CH_3CN) using hybrid functional B3LYP[8] implemented in the Gaussian 09 code.[9] We applied the 6-31G** basis sets for nonmetal atoms,[10] and Stuttgart relativistic small core 1997 effective core potential and associated basis sets for Pu.[11] Geometry was fully optimized in the gas phase. Harmonic frequency calculations were performed to confirm that the optimized structure was the stationary point on the potential energy surface. For each molecule, a subsequent single point using the implicit CPCM solvation model [12] with the Universal Force Field (UFF) radii [13] and Solvent Excluding Surface (SES)[14] was calculated to account or the solvation effects. A relatively permittivity of 35.688 was assumed in the solvation calculations to simulate CH_3CN as the solvent experimentally used for all the cases. To obtain more accurate reaction energies, in the solvation calculations we applied a larger basi set 6-311G** for nonmetal atoms,[15] and Stuttgart energy-consistent relativistic pseudopotentials ECP60MWB and associated ECP60MWB-SEG basis[16] for Pu. The used functional and basis sets have been extensively employed for actinide and lanthanide system and shown to give good agreement with experiment.[17]

Figure S12. The singly occupied natural orbitals of $[Pu^{III}(CyMe_4\text{-}BTPhen)_2(NO_3)]^{2+}$. And percent Pu(5f) character obtained from a Mulliken decomposition of the natural orbital. The contour value is 0.02 au.

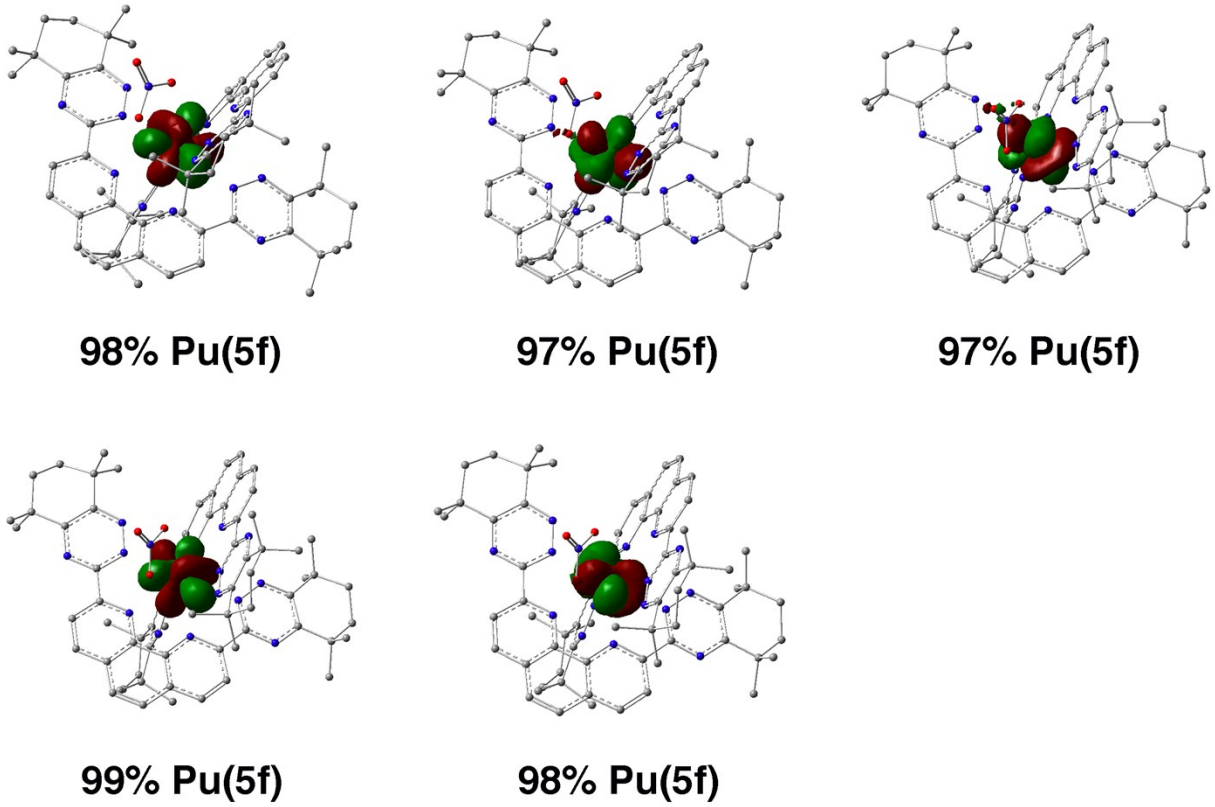

Figure S13. The singly occupied natural orbitals of $[Pu^{IV}(CyMe_4\text{-}BTPhen)_2(NO_3)]^{3+}$. And percent Pu(5f) character obtained from a Mulliken decomposition of the natural orbital. The contour value is 0.02 au.

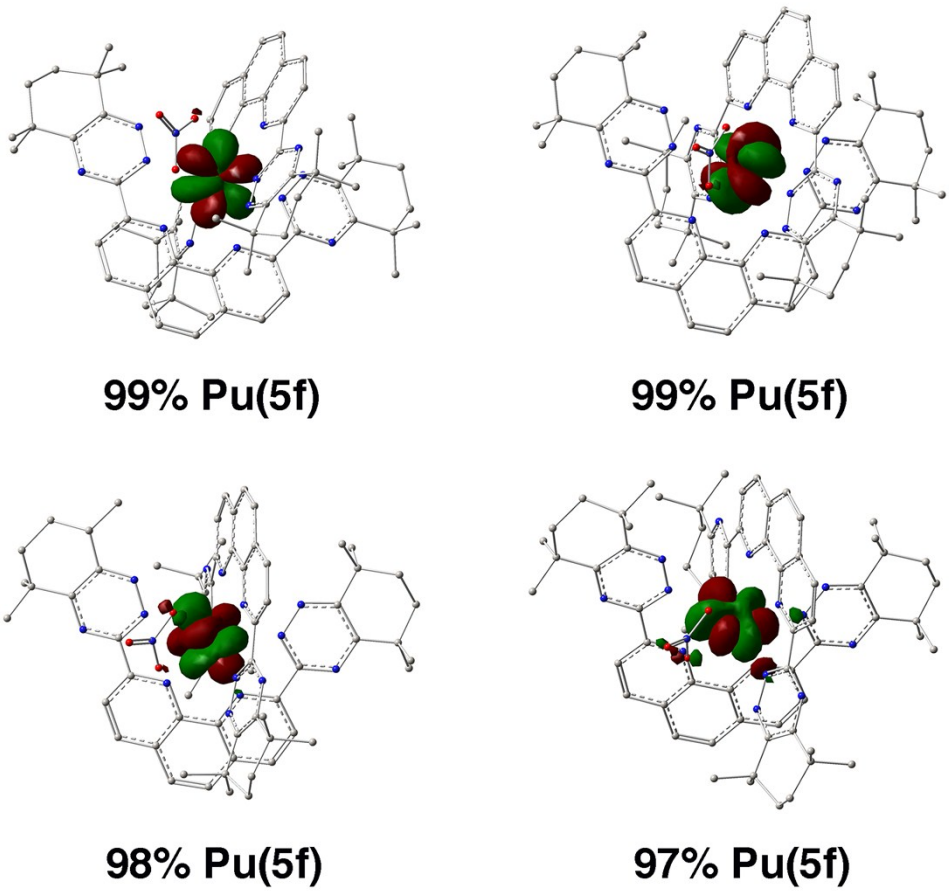

Calculation Results and Discussion: We have carried out DFT calculations on Pu(IV) complex, $Pu^{IV}(CyMe_4BTPhen)_2(NO_3)^{3+}$. Mulliken population analysis for $Pu^{IV}(CyMe_4BTPhen)_2(NO_3)^{3+}$ based on canonical orbitals shows a net spin density of 4.29 on Pu center along with a negative spin density of 0.23e on the two $CyMe_4BTPhen$ ligands. Compared to $Pu^{III}(CyMe_4BTPhen)_2(NO_3)^{2+}$ with a spin density of 5.06 on Pu center, this seems to indicate that the Pu(IV) compound is not as stable as the Pu(III) one electronically. To validate the canonical orbital picture, the natural orbitals of $Pu^{IV}(CyMe_4BTPhen)_2(NO_3)^{3+}$ were calculated. . We have added Figure S13 to the SI document showing the natural orbitals for the Pu(IV) complex, along with the previously included Figure S12 that has the natural orbitals for the Pu(III) compound. The natural orbitals provide a cleaner picture of the unpaired spin density than the canonical orbitals. The singly occupied natural orbitals in Figure S13 show that the four unpaired electrons in the Pu(IV) complex are over 97% localized on Pu 5f orbitals with no electron occupations on ligand orbitals, similar to that of Pu(III) compound in Figure S12. Based on the natural orbitals the spin density at the Pu center is 3.94 in Pu(IV) compound and 4.92 in Pu(III) one, consistently with the formal charges. Therefore, the Pu(IV)-$CyMe_4BTPhen$ compound, $Pu^{IV}(CyMe_4BTPhen)_2(NO_3)^{3+}$, is calculated to be electronically as stable as is the Pu(III)-$CyMe_4BTPhen$ compound, $Pu^{III}(CyMe_4BTPhen)_2(NO_3)^{2+}$. Therefore, the relative stability of $Pu^{III}(CyMe_4BTPhen)_2(NO_3)^{2+}$ and $Pu^{IV}(CyMe_4BTPhen)_2(NO_3)^{3+}$ dependos on the electron source for the reduction.

However, in an effort to understand the experimental observations we tested two hypotheses for possible reducing agents, namely the ligand itself, $CyMe_4BTPhen$ or the solvent molecule CH_3CN, and also a mechanism of disproportionation of Pu(IV):

Table S2. Reaction Gibbs free energies (ΔG in kcal/mol) of postulated complexation and redox reactions in CH_3CN solution.

Reactions	ΔG
(1) $[Pu^{IV}(NO_3)_6]^{2-} + 2\ CyMe_4BTPhen \rightarrow [Pu^{IV}(CyMe_4BTPhen)_2(NO_3)]^{3+} + 5\ NO_3^-$	48.7
(2) $[Pu^{IV}(CyMe_4BTPhen)_2(NO_3)]^{3+} + CyMe_4BTPhen \rightarrow [Pu^{III}(CyMe_4BTPhen)_2(NO_3)]^{2+} + CyMe_4BTPhen^+$	3.1
(3) $[Pu^{IV}(CyMe_4BTPhen)_2(NO_3)]^{3+} + CH_3CN \rightarrow [Pu^{III}(CyMe_4BTPhen)_2(NO_3)]^{2+} + CH_3CN^+$	71.1

1. $CyMe_4BTPhen/CH_3CN$ as reducing agents. The calculated thermodynamic results of possible complexation and redox reactions in the Pu-$CyMe_4BTPhen$ system are shown in Table S2. The ΔG value of complexation of $[Pu^{IV}(NO_3)_6]^{2-}$ with $CyMe_4BTPhen$ to form $Pu^{IV}(CyMe_4BTPhen)_2(NO_3)^{3+}$ (see Reaction 1 in Table S2) is +48.7 kcal/mol, which is thermodynamically unfavorable. If $CyMe_4BTPhen$ is the reducing ligand, the ΔG of the reduction of $[Pu^{IV}(CyMe_4BTPhen)_2(NO_3)]^{3+}$ by $CyMe_4BTPhen$ (see Reaction 2 in Table S2) is +3.1 kcal/mol. This very small positive ΔG value compared to that of Reaction 1 indicates that once the $Pu^{IV}(CyMe_4BTPhen)_2(NO_3)^{3+}$ is formed in solution, the reduction by 'free' $CyMe_4BTPhen$ is possible. On the other hand, considering the solvent CH_3CN as the reducing agent, the ΔG of Reaction 3 in Table S2 is +71.1 kcal/mol, which is very unfavorable. Therefore, $CyMe_4BTPhen$ ligand in solution is a possible source of reduction, but clearly more studies would be required to validate this possibility. There may also be other species or impurities in solution that could influence the redox chemistry.

2. Disproportionation of Pu(IV). It is known that Pu(IV) in acidic aqueous solution can spontaneously undergo the disproportionation reaction: $2\ Pu^{4+} + 2\ H_2O \rightarrow Pu^{3+} + PuO_2^+ + 4\ H^+$. Therefore, it is possible that water present in the CH_3CN reaction solutions facilitates disproportionation and acts a source of Pu^{3+} for complexation to the $CyMe_4BTPhen$ ligand. Such conditions would be relevant to solvent extractions, for which the organic phase is not completely anhydrous in a strict sense.

Table S3. Cartesian coordinates (in Å) of optimized geometries of Pu complexes.

$[Pu^{III}(CyMe_4\text{-}BTPhen)_2(NO_3)]^{2+}$				$[Pu^{IV}(CyMe_4\text{-}BTPhen)_2(NO_3)]^{3+}$			
C	2.19607200	-2.49415300	4.40507100	C	2.03576300	-2.90978200	4.10219700
C	2.09314200	2.32383700	-4.23050700	C	2.17610200	2.58211600	-3.87605300
Pu	-0.03257700	-0.44442800	-0.08919600	Pu	-0.07453200	-0.48083200	-0.14145200
N	1.22256800	-1.18302800	2.13320700	N	1.09592300	-1.40757900	1.93584000
O	0.20941100	-2.37338500	-1.72315700	O	0.25766600	-2.05567500	-2.04140900
O	0.05010500	-2.93552100	0.36433600	O	0.11939600	-2.88818200	-0.05962000
N	0.84723800	1.09426200	-2.04510800	N	0.87744600	1.13481600	-1.86055500
N	-1.44039700	-0.37059800	-2.35949100	N	-1.45091500	-0.15087900	-2.32120000
N	-2.46328300	-1.48587300	-0.12259700	N	-2.42239800	-1.48652100	-0.24095600
N	1.67390700	1.54862700	0.50725000	N	1.55904100	1.34652200	0.72779700
N	2.50667300	-1.32107400	-0.25531800	N	2.42190500	-1.27370000	-0.40913100
N	-1.72020000	1.71789000	-0.04691700	N	-1.58088400	1.73555700	-0.01538500
N	-1.00743500	0.40114900	2.23842500	N	-1.09219700	0.15612800	2.11979200
N	-3.33415500	2.94567100	1.17847000	N	-3.25901000	2.87788200	1.20437800
N	1.98419400	1.84833200	1.76755200	N	1.76635400	1.54369300	2.02938800
C	-0.85070800	0.13828200	-3.46162200	C	-0.84022000	0.43605900	-3.37286500
N	3.12751000	-1.35426700	-1.43176000	N	3.05578900	-1.18231800	-1.57595700
C	0.57468400	-1.06623100	3.31316900	C	0.41829200	-1.41415600	3.10726800
N	-1.96670500	2.44963800	-1.13375000	N	-1.69673400	2.60672000	-1.02089000
N	0.18184500	-3.32347400	-0.85684200	N	0.24940600	-3.12609000	-1.33080200
N	-2.92942000	-2.03443100	0.99739400	N	-2.80452000	-2.21772000	0.80814700
N	3.31102100	3.06139000	-0.29128700	N	3.27888600	2.87296700	0.18041800
O	0.27470600	-4.49262500	-1.16393800	O	0.35174800	-4.23392900	-1.78112500
C	-2.38772700	2.00570300	1.07832000	C	-2.33593700	1.92312000	1.07667000
C	2.32525400	2.17806300	-0.48065500	C	2.29046200	2.04291200	-0.15464900
C	-2.73781900	1.50368500	3.50554100	C	-2.84081200	1.18506500	3.41961600
C	2.55040800	2.54189200	-2.94878300	C	2.60766200	2.65532600	-2.56653400
C	3.64352300	3.36919600	0.95937000	C	3.52533200	3.07247800	1.47305000
C	2.33787700	-1.91455800	2.07939900	C	2.23741000	-2.09766100	1.84811500
C	1.89422200	1.90703900	-1.87430400	C	1.92616800	1.91699700	-1.58095200
C	3.03371800	-2.00074900	0.77146100	C	2.96482600	-2.02123200	0.56393300
C	1.02507400	-1.71106700	4.49689600	C	0.84549000	-2.16066900	4.23545600
C	-2.56000800	-1.08238100	-2.49813900	C	-2.61318800	-0.77996000	-2.52041800
C	-4.03341700	-2.78164600	0.96682800	C	-3.92231000	-2.93778300	0.74358900
C	-1.38425100	-0.04773100	-4.76588700	C	-1.39031800	0.42207200	-4.68209300
C	-1.25775500	-0.04088100	4.61929500	C	-1.44180200	-0.49614000	4.44148300
C	-0.59990400	-0.22139600	3.37115800	C	-0.74522400	-0.57668400	3.20741300
C	-3.60161900	3.68127700	0.10363700	C	-3.40680500	3.74951400	0.21080200
N	4.14041400	-2.74553400	0.69443100	N	4.10869700	-2.69390500	0.44338700
C	0.35661400	0.91927400	-3.29530500	C	0.39854600	1.12386400	-3.12763200
C	-2.03126300	1.25706000	2.31007100	C	-2.09117900	1.03889900	2.23613900
C	2.93446500	2.74698000	2.03176800	C	2.69965800	2.40388400	2.43856200
C	-2.57622300	-0.79498900	-4.88056200	C	-2.62816200	-0.23379400	-4.85879700
C	-2.86739000	3.43352300	-1.09620500	C	-2.55484300	3.62423400	-0.93831500
C	4.74867500	-2.83627100	-0.48598400	C	4.74502900	-2.65426800	-0.72557000
N	-4.25813100	-2.39182800	-1.36855900	N	-4.33209600	-2.13500900	-1.46729400
C	2.86050100	-2.58979500	3.20207800	C	2.74138900	-2.86479500	2.91725200
C	0.96021600	1.50878600	-4.43989300	C	1.03012800	1.82037400	-4.19149900
C	-3.17027700	-1.31054800	-3.74883000	C	-3.24598900	-0.83013100	-3.77713600
C	-3.13236300	-1.67858800	-1.26678900	C	-3.16835300	-1.49495500	-1.35398100
C	-4.72758000	-2.97480900	-0.26850000	C	-4.74994700	-2.86383900	-0.43416900
C	4.23062600	-2.08882600	-1.58749500	C	4.19244100	-1.85152600	-1.77941200
C	-2.35867300	0.84108300	4.65238300	C	-2.52719300	0.40399800	4.51360200

C	0.30663000	-1.53790700	5.72562600	C	0.08506300	-2.10173000	5.45104600
C	-0.72013000	0.52718100	-5.89935300	C	-0.68951100	1.07804500	-5.74915500
C	-0.78904000	-0.73094100	5.78564600	C	-1.01240500	-1.29809600	5.55139500
C	3.17611500	3.08115200	3.50198300	C	2.80667900	2.65892600	3.93873800
C	-4.45682300	-3.43611300	2.27853600	C	-4.23526400	-3.86128800	1.91408400
C	4.79782600	4.34104900	1.16348400	C	4.70345600	3.95723700	1.84257900
C	0.40488200	1.27913800	-5.74217400	C	0.47100300	1.75381900	-5.51233100
C	-6.01186300	-3.78204800	-0.39480500	C	-6.10958900	-3.52840100	-0.54249800
C	4.55273200	3.77049100	3.65549600	C	4.19808900	3.25552300	4.26217100
C	3.15062500	1.80454000	4.36640500	C	2.61539800	1.35733400	4.74154300
C	-5.95271800	-4.68193800	-1.64808200	C	-6.30204100	-4.14443400	-1.94574500
C	2.03455400	4.02243300	3.96583700	C	1.67930000	3.65524300	4.32089900
C	4.67715600	5.52884400	0.18528600	C	4.74831100	5.20565900	0.93485200
C	-3.50016600	-4.63014500	2.53471000	C	-3.37647500	-5.14208600	1.72181500
C	6.10831400	3.56823600	0.85376100	C	5.98851000	3.11448200	1.60034200
C	4.79983400	4.86659800	2.61773000	C	4.60424200	4.39224000	3.32323600
C	-4.33607600	-2.43979900	3.44899600	C	-3.86175500	-3.20843000	3.25823600
C	-5.92265800	-3.91747600	2.16800300	C	-5.74432100	-4.20438200	1.91103000
C	-6.06076400	3.94504500	0.18816800	C	-5.84862100	4.06355800	0.05163100
C	-3.02643300	4.27323500	-2.36180000	C	-2.54917900	4.64186300	-2.07573900
C	-4.71321800	4.71588900	0.21522300	C	-4.50395400	4.79170000	0.33882200
C	-4.60296200	5.47975800	1.55174100	C	-4.54368200	5.36295400	1.77284000
C	5.99325100	-3.70874400	-0.57020700	C	6.04470900	-3.43023900	-0.84756300
C	4.84378400	-2.11405200	-2.98455500	C	4.81147300	-1.76697400	-3.17024600
C	-4.62788200	5.71596100	-0.96078400	C	-4.27258400	5.93784600	-0.67255000
C	-4.36885400	5.04081300	-2.30840600	C	-3.87385700	5.44310100	-2.06299300
C	-3.00402700	3.38378200	-3.62064500	C	-2.39422400	3.95111100	-3.44422500
C	-7.17747800	-2.76955900	-0.55821000	C	-7.16603200	-2.40233100	-0.33920400
C	-6.21684900	-4.65832100	0.86258900	C	-6.26578300	-4.62539300	0.53637100
C	5.73815200	-5.06040400	0.13177100	C	5.88205700	-4.84067800	-0.23772200
C	-1.83131400	5.25947000	-2.42475900	C	-1.33643400	5.58347500	-1.84666800
C	6.36935100	-3.95600300	-2.04951500	C	6.46242100	-3.54801300	-2.33167700
C	7.13450600	-2.96427400	0.17288300	C	7.11612200	-2.65081200	-0.03302800
C	3.93347100	-2.99354600	-3.88082300	C	3.97019700	-2.67724600	-4.10564200
C	6.27501000	-2.69639600	-2.91236200	C	6.28188900	-2.24590500	-3.11268600
C	4.90320100	-0.69088300	-3.57610700	C	4.76783900	-0.32311500	-3.70708300
H	-8.11443900	-3.31644000	-0.69918100	H	-8.16518200	-2.83252500	-0.45115300
H	-7.29253900	-2.12230500	0.31655400	H	-7.10470400	-1.94477800	0.65271100
H	-7.01597300	-2.13459900	-1.43392700	H	-7.04576000	-1.61701200	-1.09079200
H	-5.10490100	-5.37296500	-1.60343300	H	-5.53385200	-4.89321300	-2.16278200
H	-6.86881000	-5.27700600	-1.70730000	H	-7.27476300	-4.64240700	-1.98387200
H	-5.86722000	-4.09165900	-2.56248700	H	-6.27731500	-3.38422400	-2.72863800
H	-3.30214900	-2.12335300	3.59752500	H	-2.78790600	-3.02510000	3.33110700
H	-4.95011700	-1.54879100	3.27892900	H	-4.38961300	-2.25950300	3.40124800
H	-4.68699000	-2.91879900	4.36841800	H	-4.15015500	-3.87858700	4.07320500
H	-3.55932700	-5.38694400	1.74744400	H	-3.59889800	-5.66016800	0.78503100
H	-2.46308000	-4.28692100	2.58805600	H	-2.31018100	-4.89648000	1.72488800
H	-3.75879000	-5.11007800	3.48396500	H	-3.57390300	-5.83709500	2.54350700
H	1.06327200	3.53266900	3.84678600	H	0.69645800	3.22963700	4.09441100
H	2.16730300	4.27059500	5.02353400	H	1.72346400	3.86325000	5.39411000
H	2.01146700	4.95910800	3.40116500	H	1.76535700	4.60839000	3.79168200
H	3.90160100	1.08170400	4.03066200	H	3.34708900	0.59688600	4.44916500
H	3.37741900	2.06620800	5.40462800	H	2.75947200	1.56752200	5.80533200
H	2.17242400	1.32135900	4.33838700	H	1.61335100	0.94473300	4.60816400
H	6.09241900	3.17833600	-0.16801700	H	6.04914000	2.79257200	0.55676000
H	6.96079900	4.24737800	0.94832700	H	6.86475500	3.73130300	1.81874300

H	6.26789800	2.72867800	1.53704300	H	6.03309900	2.22716000	2.23882000
H	4.72896400	5.20008800	-0.85443100	H	4.89192800	4.93865000	-0.11384100
H	3.73620200	6.06992300	0.32908900	H	3.83049600	5.79605400	1.02081700
H	5.49770700	6.22946500	0.36572500	H	5.58363600	5.84045600	1.24300500
H	8.03328900	-3.58802400	0.17399000	H	8.05686700	-3.20770200	-0.06011900
H	7.38625000	-2.01028700	-0.30030700	H	7.30375400	-1.65198600	-0.43806200
H	6.85314000	-2.76647000	1.21103600	H	6.80997500	-2.54754500	1.01174700
H	6.62924700	-5.68833000	0.03902000	H	6.81723100	-5.39300400	-0.36487300
H	5.52139900	-4.92622300	1.19342800	H	5.65492900	-4.79610000	0.82924100
H	4.89987100	-5.59545400	-0.32569300	H	5.08932100	-5.40489800	-0.73904900
H	5.38068500	-0.72792800	-4.56027800	H	5.26167000	-0.28839700	-4.68260000
H	3.90471400	-0.26535800	-3.69203600	H	3.74108200	0.02614900	-3.82942100
H	5.49389700	-0.02032400	-2.94239000	H	5.29572600	0.36779900	-3.04096400
H	3.87503900	-4.02647500	-3.52634300	H	3.97543200	-3.72312200	-3.78672000
H	2.91612500	-2.59318500	-3.90475300	H	2.92965200	-2.34103000	-4.13782100
H	4.32841100	-3.00865000	-4.90169100	H	4.38057700	-2.63401400	-5.11901800
H	5.71708900	-4.73604400	-2.45946000	H	5.88587300	-4.35091400	-2.80519500
H	7.38549300	-4.36208500	-2.08655800	H	7.50865200	-3.86622000	-2.37177300
H	6.61296400	-2.91322300	-3.93118800	H	6.64253200	-2.37225000	-4.13839000
H	6.95586100	-1.92856500	-2.52404100	H	6.89985100	-1.45507200	-2.66981500
H	5.34135000	3.01089800	3.58853300	H	4.94681900	2.45480000	4.22630900
H	4.62081600	4.18852300	4.66539600	H	4.18752500	3.61251100	5.29690900
H	5.76074400	5.35499800	2.80975100	H	5.57256000	4.79997200	3.62924400
H	4.03881600	5.64991700	2.71647400	H	3.89063700	5.22008300	3.40716700
H	-3.83694400	6.44648800	-0.75283900	H	-3.50338500	6.61313300	-0.28000200
H	-5.56143800	6.28662100	-1.00066500	H	-5.18878100	6.53277900	-0.73700000
H	-5.18596700	4.34625900	-2.53924600	H	-4.67277400	4.81855900	-2.48077000
H	-4.37271000	5.78837300	-3.10867700	H	-3.76771000	6.29262900	-2.74507500
H	-0.88466800	4.71136800	-2.45559900	H	-0.40041600	5.01601800	-1.85953100
H	-1.90436800	5.87072200	-3.32973900	H	-1.29650300	6.32889700	-2.64650800
H	-1.80228600	5.93474400	-1.56458800	H	-1.39550400	6.11794300	-0.89432000
H	-2.04331500	2.88019600	-3.73866300	H	-1.43207400	3.44417900	-3.53401600
H	-3.78997200	2.62219400	-3.58408300	H	-3.19142100	3.22004200	-3.61426600
H	-3.17900700	4.00471700	-4.50474800	H	-2.45810500	4.70430600	-4.23495000
H	-4.07964900	-1.89594200	-3.79188900	H	-4.19062200	-1.35186200	-3.86901400
H	-3.01475900	-0.96043100	-5.86025000	H	-3.08526300	-0.26871000	-5.84325700
H	-1.13918300	0.35928300	-6.88677100	H	-1.11111600	1.04029700	-6.74874100
H	0.89723000	1.72420400	-6.60141000	H	0.98443800	2.26646600	-6.31980900
H	2.58531100	2.78827200	-5.08010300	H	2.69352900	3.12864100	-4.65909200
H	3.39519100	3.18560500	-2.74165600	H	3.45150000	3.26659400	-2.27271900
H	3.76544700	-3.17246300	3.08895600	H	3.66829000	-3.40682300	2.77861900
H	2.56858200	-3.00898400	5.28582700	H	2.39676200	-3.50328300	4.93699700
H	0.66301200	-2.05350800	6.61218200	H	0.41266100	-2.69574000	6.29855500
H	-1.32184500	-0.58922800	6.72092200	H	-1.57123300	-1.24139100	6.48028000
H	-2.88935000	1.00290900	5.58616400	H	-3.09285400	0.49472800	5.43637700
H	-3.55714200	2.21033600	3.49432900	H	-3.63812700	1.91685600	3.44522000
H	-3.63927100	5.99188900	1.64018400	H	-3.59017500	5.82630700	2.04569100
H	-5.39082300	6.23715200	1.60031100	H	-5.31727000	6.13381000	1.82767100
H	-4.71641600	4.81146400	2.40746400	H	-4.77815600	4.59240200	2.50968200
H	-6.10743000	3.22275700	1.00824500	H	-6.00314000	3.24301400	0.75818800
H	-6.88602500	4.65319200	0.30803800	H	-6.67046700	4.77524300	0.17021300
H	-6.21291100	3.40484600	-0.75105200	H	-5.89732700	3.65823600	-0.96332700
H	-6.13995300	-4.56548900	3.02363200	H	-5.91553200	-5.00705400	2.63527500
H	-6.59199600	-3.05340100	2.26418900	H	-6.30927000	-3.33878000	2.27848300
H	-7.24768300	-5.02729500	0.86421900	H	-7.32495900	-4.89145800	0.60532600
H	-5.57848200	-5.54647500	0.78809100	H	-5.74982200	-5.53268700	0.20264000

$[Pu^{IV}(NO_3)_6]^{2-}$				
Pu	0.00000000	0.00000000	-0.00000200	
O	2.47809700	-0.32147400	-0.32522700	
O	1.36170300	-2.11855400	0.08246200	
O	3.52789500	-2.24183100	-0.22279000	
O	-1.33686300	-2.04155700	-0.62656000	
O	-2.16930900	-3.49153700	0.78947800	
O	-1.02362600	-1.75887500	1.48631800	
O	0.57667400	-0.87596000	-2.29090400	
O	-0.60916800	-0.54966900	-4.10406700	
O	-1.23965400	0.27707800	-2.17541400	
N	2.49616100	-1.58634200	-0.15826800	
N	-1.53475200	-2.47063700	0.55874300	
N	-0.43155300	-0.38991700	-2.90351900	
O	-2.47809900	0.32147400	0.32522200	
O	-1.36170400	2.11855400	-0.08246200	
O	-3.52789900	2.24182800	0.22276500	
O	1.33686400	2.04155500	0.62656000	
O	2.16931000	3.49153700	-0.78947600	
O	1.02362600	1.75887700	-1.48631900	
O	-0.57667600	0.87595900	2.29090200	
O	0.60916500	0.54966600	4.10406600	
O	1.23965400	-0.27707700	2.17541200	
N	-2.49615100	1.58635000	0.15833400	
N	1.53475300	2.47063600	-0.55874300	
N	0.43155300	0.38991700	2.90351700	

References

(1) Cohen, D. *J. Inorg. Nucl. Chem.* **1961,** *18*, 211.

(2) (a) Lewis, F. W.; Harwood, L. M.; Hudson, M. J.; Drew, M. G. B.; Desreux, J. F.; Vidick, G.; Bouslimani, N.; Modolo, G.; Wilden, A.; Sypula, M.; Vu, T.-H.; Simonin, J.-P. *J. Am. Chem. Soc.* **2011**, *133*, 13093. (b) Whittaker, D. M.; Griffiths, T. L.; Helliwell, M.; Swinburne, A. N.; Natrajan, L. S.; Lewis, F. W.; Harwood, L. M.; Parry, S. A.; Sharrad, C. A. *Inorg. Chem.* **2013**, *52*, 3429.

(3) Bremer, A.; Whittaker, D. M.; Sharrad, C. A.; Geist,, A.; Panak, P. J. *Dalton Trans.* **2014**, *43*, 2684.

(4) SMART 4.210, **1996**, Bruker AXS, Inc., Madison, Wisconsin 53719.

(5) SAINT 5.050, **1998**, Bruker AXS, Inc., Madison, Wisconsin 53719.

(6) SADABS, 2.03, **2001** George Sheldrick, University of Göttingen, Germany.

(7) SHELXTL Version 6.10, **2001**, Bruker AXS, Inc., Madison, Wisconsin 53719.

(8) (a) Becke, A. D. *J. Chem. Phys.* **1993**, *98*, 5648. (b) Lee, C.; Yang, W.; Parr, R. G. *Phys. Rev. B* **1988**, *37*, 785.

(9) Frisch, M. J.; Trucks, G. W.; Schlegel, H. B.; Scuseria, G. E.; Robb, M. A.; Cheeseman, J. R.; Scalmani, G.; Barone, V.; Mennucci, B.; Petersson, G. A.; Nakatsuji, H.; Caricato, M.; Li, X.; Hratchian, H. P.; Izmaylov, A. F.; Bloino, J.; Zheng, G.; Sonnenberg, J. L.; Hada, M.; Ehara, M.; Toyota, K.; Fukuda, R.; Hasegawa, J.; Ishida, M.; Nakajima, T.; Honda, Y.; Kitao, O.; Nakai, H.; Vreven, T.; Montgomery, J. A., Jr.; Peralta, J. E.; Ogliaro, F.; Bearpark, M.; Heyd, J. J.; Brothers, E.; Kudin, K. N.; Staroverov, V. N.; Kobayashi, R.; Normand, J.; Raghavachari, K.; Rendell, A.; Burant, J. C.; Iyengar, S. S.; Tomasi, J.; Cossi, M.; Rega, N.; Millam, J. M.; Klene,

M.; Knox, J. E.; Cross, J. B.; Bakken, V.; Adamo, C.; Jaramillo, J.; Gomperts, R.; Stratmann, R. E.; Yazyev, O.; Austin, A. J.; Cammi, R.; Pomelli, C.; Ochterski, J. W.; Martin, R. L.; Morokuma, K.; Zakrzewski, V. G.; Voth, G. A.; Salvador, P.; Dannenberg, J. J.; Dapprich, S.; Daniels, A. D.; Farkas, Ö.; Foresman, J. B.; Ortiz, J. V.; Cioslowski, J.; Fox, D. J. Gaussian 09, revision D.01; Gaussian Inc.: Wallingford, CT, 2013.

(10) Hariharan, P.C.; Pople, J. A. *Theoret. Chimica Acta* **1973**, *28*, 213

(11) Küchle, W.; Dolg, M.; Stoll, H.; Preuss, H. *J. Chem. Phys.* **1994**, *100*, 7535.

(12) Cossi, M.; Rega, N.; Scalmani, G.; Barone, V. Energies, structures, and electronic properties of molecules in solution with the C-PCM solvation model. J. Comput. Chem. 2003, 24, 669−681.

(13) Rappe, A. K.; Casewit, C. J.; Colwell, K. S.; Goddard, W. A.; Skiff, W. M. *J. Am. Chem. Soc.* 1992, *114*, 10024.

(14) (a) Connolly, M. L. J. Mol. Graphics **1993**, *11*, 139. (b) Connolly, M. L. *J. Appl. Crystallogr.* **1983**, *16*, 548.

(15) Krishnan, R.; Binkley, J. S.; Seeger, R.; Pople, J. A. *J. Chem. Phys.* **1980**, *72*, 650.

(16) (a) Cao, X.; Dolg, M. *J. Mol. Struct.: THEOCHEM* **2004**, *673*, 203. (b) Cao, X.; Dolg, M.; Stoll, H. *J. Chem. Phys.* **2003**, *118*, 487−496.

(17) (a) Su, J.; Windorff, C. J.; Batista, E. R.; Evans, W. J.; Gaunt, A. J.; Janicke, M. T.; Kozimor, S. A.; Scott, B. L.; Woen, D. H.; Yang, P. J. Am. Chem. Soc. 2018, DOI: 10.1021/jacs.8b03907. (b) McSkimming, A.; Su, J.; Cheisson, T.; Gau, M. R.; Carroll, P. J.; Batista, E. R.; Yang, P.; Schelter, E. J. *Inorg. Chem.* **201**8, *57*, 4387. (c) Cross, J. N.; Su, J.; Batista, E. R.; Cary, S. K.; Evans, W. J.; Kozimor, S. A.; Mocko, V.; Scott, B. L.; Stein, B. W.; Windorff, C. J.; Yang, P. *J. Am. Chem. Soc.* **2017**, *139*, 8667. (d) Fieser, M. E.; Ferrier, M. G.; Su, J.; Batista, E. R.; Cary, S.

K.; Engle, J. W.; Evans, W. J.; Lezama Pacheco, J. S.; Kozimor, S. A.; Olson, A. C.; Ryan, A. J.; Stein, B. W.; Wagner, G. L.; Woen, D. H.; Vitova, T.; Yang, P. *Chem. Sci*. **2017**, *8*, 6076 (e) Minasian, S. G.; Keith, J. M.; Batista, E. R.; Boland, K. S. *Chem. Sci.* **2014**, *5*, 351. (f) Spencer, L. P.; Yang, P.; Minasian, S. G.; Jilek, R. E.; Batista, E. R.; Boland, K. S.; Boncella, J. M.; Conradson, S. D.; Clark, D. L.; Hayton, T. W.; Kozimor, S. A.; Martin, R. L.; MacInnes, M. M.; Olson, A. C.; Scott, B. L.; Shuh, D. K.; Wilkerson, M. P. *J. Am. Chem. Soc.* **2013**, *135*, 2279. (g) Minasian, S. G.; Keith, J. M.; Batista, E. R.; Boland, K. S.; Clark, D. L.; Conradson, S. D.; Kozimor, S. A.; Martin, R. L.; Schwarz, D. E.; Shuh, D. K.; Wagner, G. L.; Wilkerson, M. P.; Wolfsberg, L. E.; Yang, P. *J. Am. Chem. Soc.* **2012**, *134*, 5586. (h) Keith, J.M.; Batista, E.R. *Inorg. Chem.* **2012**, *51*, 13. (i) Kozimor, S. A.; Yang, P.; Batista, E. R.; Boland, K. S.; Burns, C. J.; Clark, D. L.; Conradson, S. D.; Martin, R. L.; Wilkerson, M. P.; Wolfsberg, L. E. *J. Am. Chem. Soc.* **2009**, *131*, 12125.